

Coupled Sublattice Melting and Charge-Order Transition in Two Dimensions

T. S. Smith^{1,*}, F. Ming^{2,*}, D. G. Trabada³, C. Gonzalez³, D. Soler-Polo³, F. Flores³,
J. Ortega³, and H. H. Weitering^{1,†}

¹*Department of Physics and Astronomy, The University of Tennessee, Knoxville, Tennessee 37996, USA*

²*State Key Laboratory of Optoelectronic Materials and Technologies, School of Electronics and Information Technology and Guangdong Province Key Laboratory of Display Material, Sun Yat-sen University, Guangzhou 510275, China*

³*Departamento de Física Teórica de la Materia Condensada and Condensed Matter Physics Center (IFIMAC), Universidad Autónoma de Madrid, ES-28049 Madrid, Spain*

 (Received 17 December 2019; accepted 28 January 2020; published 2 March 2020)

Two-dimensional melting is one of the most fascinating and poorly understood phase transitions in nature. Theoretical investigations often point to a two-step melting scenario involving unbinding of topological defects at two distinct temperatures. Here, we report on a novel melting transition of a charge-ordered K-Sn alloy monolayer on a silicon substrate. Melting starts with short-range positional fluctuations in the K sublattice while maintaining long-range order, followed by longer-range K diffusion over small domains, and ultimately resulting in a molten sublattice. Concomitantly, the charge order of the Sn host lattice collapses in a multistep process with both displacive and order-disorder transition characteristics. Our combined experimental and theoretical analysis provides a rare insight into the atomistic processes of a multistep melting transition of a two-dimensional materials system.

DOI: [10.1103/PhysRevLett.124.097602](https://doi.org/10.1103/PhysRevLett.124.097602)

Two-dimensional (2D) materials are fundamentally different from 3D solids. This difference is especially manifest in phase transitions and critical phenomena as the balance between energy and entropy is profoundly altered in low dimension. The melting transition provides a striking contrast. 3D melting is known to be a first order phase transition. Conversely, 2D melting transitions are believed to be continuous and topological in nature [1–5]. Structural phase transitions, however, are often described within Landau’s conceptual framework of spontaneous symmetry breaking [6,7]. They can be continuous or discontinuous. Examples include the ubiquitous charge-order transitions in (quasi) 2D materials, surfaces, and interfaces. Symmetry and dimensionality are the quintessential ingredients of this theoretical framework.

Here, we report on a novel phase transition in a charge-ordered K-Sn alloy monolayer (ML) on Si(111), whereby the “melting” of the charge order in the Sn host lattice is preceded and driven by a true 2D melting transition in the K sublattice. Sublattice melting is a well-known phenomenon in bulk ionic conductors where an ionic insulator acquires a highly conductive state when the sublattice containing the lighter ions, typically an alkali or Ag ion, melts while the heavier sublattice or “host” lattice remains intact [8,9]. A similar part-liquid part-crystalline state has been observed in thermoelectric compounds with strong chemical-bond hierarchy [10]. Here, we show that sublattice melting can happen in 2D and that it can have profound consequences for the charge-order transition in the 2D host lattice. Specifically, the phase transition in the K-Sn adatom

system turns out to be a multistep process involving two intermediate regimes. The first is characterized by short-range positional fluctuations in the K sublattice and partial band gap reduction of the charge-ordered condensate. The second involves longer-range diffusion of the K atoms, the nucleation of liquidlike islands, and quenching of charge ordering in the Sn host lattice. The latter involves both a displacive and order-disorder mechanism. The present study provides a rare glimpse into the atomistic processes of a 2D melting transition, which remains one of the oldest outstanding problems in condensed matter physics [4,5].

Potassium was deposited from a SAES getter source onto the Si(111)($\sqrt{3} \times \sqrt{3}$) $R30^\circ$ -Sn surface (henceforth $\text{Sn}\sqrt{3}$) under ultrahigh vacuum. The $\text{Sn}\sqrt{3}$ surface consists of a triangular array of Sn adatoms that are located at the T_4 adsorption sites of the Si(111) surface. The coverage is $\Theta_{\text{Sn}} = 1/3$ ML [11–13]. Details can be found in Ref. [13]. The surfaces were characterized with scanning tunneling microscopy and spectroscopy (STM and STS). Film growth on n -type Si(111) produces larger domains with fewer defects, which facilitated the analysis of temperature-dependent STM images. Low-temperature STS, however, requires the use of p -type Si [14]. We used both n - and p -type substrates to verify the consistency of our results.

Figure 1 shows STM images of a well-ordered ($2\sqrt{3} \times 2\sqrt{3}$) $R30^\circ$ structure (henceforth $2\sqrt{3}$ -K) formed by evaporating K onto the $\text{Sn}\sqrt{3}$ surface at 77 K. The K coverage is $\Theta_K = 1/6$ ML and the unit cell (UC) has quadrupled relative to the $\text{Sn}\sqrt{3}$ substrate UC [15]. Here, we show the result for the heavily doped p -type substrate; the same

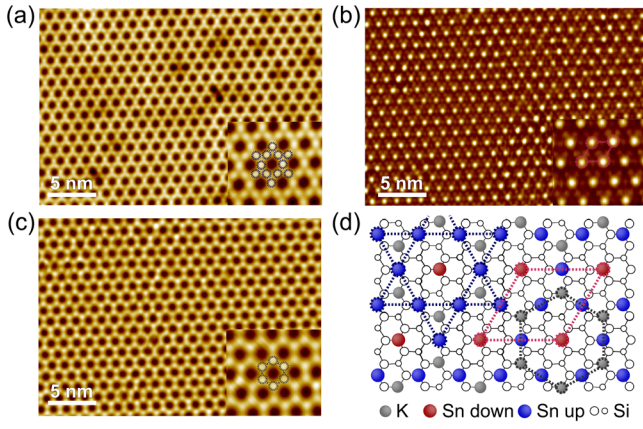


FIG. 1. STM topography of the $2\sqrt{3}$ -K structure on heavily doped *p*-type Si(111). The images, recorded at 77 K, show exactly the same surface area. Images are scanned at (a) -1.5 V and 1 nA, revealing a kagome lattice composed of the Sn up atoms; (b) 1.0 V and 1 nA revealing the triangular lattice comprised of the Sn down atoms; and (c) 2.5 V and 1 nA, showing a honeycomb lattice corresponding to the K locations. The insets in (a)–(c) are enlarged images, which more clearly reveal the corresponding sublattices. (d) The $2\sqrt{3}$ -K structure obtained from DFT calculations. The K atoms reside at the T_4 adsorption sites at the centers of the Sn “up” triangles.

structure is formed on the other substrates. The images reveal three distinct lattices, depending on the tunneling bias. The filled state image in Fig. 1(a) shows a kagome lattice with three bright adatoms and one dim atom per UC. These are the Sn adatoms (see below). The dim atoms are located at the center of each hexagon. Though hardly seen in this image, they form a bright triangular lattice in the empty state image [Fig. 1(b)]. The kagome lattice is hardly visible at this bias ($+1.0$ V). The triangular lattice fades with increased bias and a bright honeycomb lattice appears above ~ 1.3 V [Fig. 1(c)]. These are the K atoms, located at the centers of the chained triangles of the kagome lattice. STM imaging of the honeycomb lattice becomes problematic above 130 K as K atoms begin to diffuse.

Images for $\Theta_K \ll 1/6$ ML reveal that the kagome and triangular lattice sites coincide with the Sn adatom locations of the $\text{Sn}\sqrt{3}$ substrate [15]. The registry of the Sn and K atoms from the STM images is illustrated in Fig. 1(d). For $\Theta_K = 1/6$ ML, there are four Sn adatoms and two K atoms per $(2\sqrt{3} \times 2\sqrt{3})$ UC. Assuming that the K atoms are ionized, there are six valence electrons to be distributed over four Sn dangling bonds (DBs), resulting in three doubly occupied DB orbitals and one empty DB orbital. The three adatoms with doubly occupied DBs relax outward [29,30], forming the kagome sublattice. Adatoms with empty DBs relax inward, forming the triangular sublattice [29,30]. This charge-ordering phenomenon [30–32] is accompanied by a buckling distortion of the Sn adatom lattice [30]. Shown later with STS, the ground state is insulating.

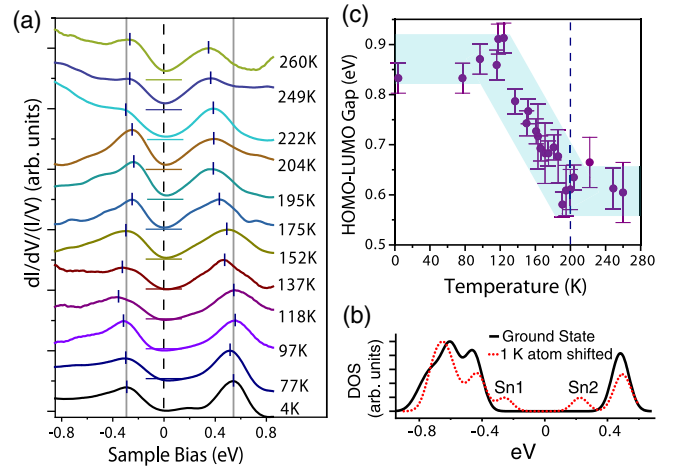


FIG. 2. Evolution of the HOMO-LUMO states. (a) Temperature dependent $dI/dV/(I/V)$ spectra of the $2\sqrt{3}$ -K structure on moderately doped *p*-type Si(111). Because of the nature of the diffusing K adatoms, spectra were obtained using weak tunneling conditions ($I_t = 30$ pA), averaging several I/V curves and differentiating. The HOMO-LUMO maxima are indicated by vertical tick marks. Gray vertical lines mark the HOMO-LUMO locations at 4 K. The reduction of the HOMO-LUMO splitting above 118 K is primarily attributed to the apparent shift of the LUMO state. Horizontal tick marks below each spectrum indicate the zero of the tunneling conductance. The increase in zero-bias conductance (ZBC) above 175 K, signals a gradual insulator-metal transition. (b) Theoretical LDOS of the $(2\sqrt{3} \times 2\sqrt{3})R30^\circ$ ground state and $(4\sqrt{3} \times 4\sqrt{3})R30^\circ$ excited-state system with one displaced K atom, producing new band gap states at about -0.25 and $+0.22$ eV. (c) Evolution of the experimental HOMO-LUMO gap, as measured from the positions of the LDOS maxima. Error bars were estimated from the small fluctuations in the HOMO-LUMO positions in different experimental runs.

This scenario is confirmed with plane-wave DFT (density functional theory) calculations using the QUANTUM ESPRESSO code [33]. The total-energy-minimized structure indicates a 0.23 Å height difference between the Sn-up and Sn-down atoms or, equivalently, between the kagome and triangular sublattices, respectively; the K honeycomb layer is located 0.75 Å above the kagome layer. STM image simulations are fully consistent with the images in Fig. 1 [15].

Figure 2(a) shows temperature-dependent normalized dI/dV spectra of the $2\sqrt{3}$ -K surface, reflecting the local density of states (LDOS) [34]. Spectra in Fig. 2(b) were calculated with DFT, using the PBE0 hybrid functional [35,36]. The ground-state spectrum [black line in Fig. 2(b)] is in good agreement with the measured spectrum at 4 K [Fig. 2(a)], although hybrid functional calculations slightly overestimate the band gap. The experimental spectrum is characterized by a DOS peak centered at about -0.3 eV, and a peak centered at about $+0.5$ eV. The highest occupied molecular orbital (HOMO) at about -0.3 eV is associated with the DB orbitals of the Sn-up atoms, as

the corresponding STM images show the kagome lattice [Fig. 1(a)]. The lowest unoccupied molecular orbital (LUMO) at about +0.5 V is associated with the Sn-down atoms of the triangular lattice. The HOMO-LUMO splitting is a measure of the Sn up-down lattice distortion in the charge-ordered $2\sqrt{3}$ -K phase. Its temperature dependence is shown in Fig. 2(c). This splitting decreases gradually, starting at 130 K and leveling off at 200 K where it reduces to about 70 percent of its original value. This decrease should be primarily attributed to the downward shift of the LUMO state, or more precisely, to the development of a shoulder on the low-energy side of the LUMO state [Fig. 2(a)]. The HOMO location remains almost constant at -0.27 ± 0.03 eV [37]. The shoulder on the LUMO side is clearly visible in the 175 K spectrum and appears to be centered near +0.2 eV. This broadening leads to a gradual insulator-metal transition near 175 K.

Figure 3 shows the temperature-dependent topography of the $2\sqrt{3}$ -K structure on the *n*-type substrate. Similar behavior is seen on *p*-type substrates [15]. At 77 K, the surface is fully covered with the $2\sqrt{3}$ -K structure. Since there are four equivalent adatom sites per $(2\sqrt{3} \times 2\sqrt{3})$ UC prior to K deposition, there are four different domains indicated with different colors. By slowly warming the sample to room temperature, small patches of the $2\sqrt{3}$ -K phases convert to a new $(\sqrt{3} \times \sqrt{3})$ lattice [gray areas in Figs. 3(b)–3(d)]. Some of the areas are not fully converted to a $(\sqrt{3} \times \sqrt{3})$ lattice and still show weak $(2\sqrt{3} \times 2\sqrt{3})$ ordering around defects [Fig. 3(d)] or a stripelike $(\sqrt{3} \times 2\sqrt{3})$ structure [Fig. 3(c), inset]. Subsequent cooling to 77 K produces a single domain $2\sqrt{3}$ -K lattice [Fig. 3(e)], indicating that K atoms diffuse over long distances during the annealing cycle.

Figure 3(f) shows the area fraction of the $2\sqrt{3}$ -K phase as a function of temperature. Below 200 K, the $2\sqrt{3}$ -K phase covers the entire surface. Above 200 K, the $(2\sqrt{3} \times 2\sqrt{3})$, $(2\sqrt{3} \times \sqrt{3})$, and $(\sqrt{3} \times \sqrt{3})$ structures coexist. The onset temperature for this phase coexistence coincides with the end point of the transition in Fig. 2(c). This can be seen from the enlarged data in the inset, most noticeably for heavily doped *p*-type silicon substrates, showing a clear reduction in the area fraction of the buckled $2\sqrt{3}$ -K phase starting at 200 K. While this reduction is slow initially, the area fraction of the $2\sqrt{3}$ -K phase drops steeply near 275 K, possibly indicating a first order phase transition to the “flat” $(\sqrt{3} \times \sqrt{3})$ phase. We tentatively conclude that there are at least two transitions. One is a continuous transition from the long-range-ordered $2\sqrt{3}$ -K phase below 130 K to the mixed phase above 200 K, accompanied by the gradual reduction of the HOMO-LUMO gap. The other is the collapse of the charge order near 275 K.

To understand the atomic mechanisms of this phase transition, we conducted DFT-MD simulations at various

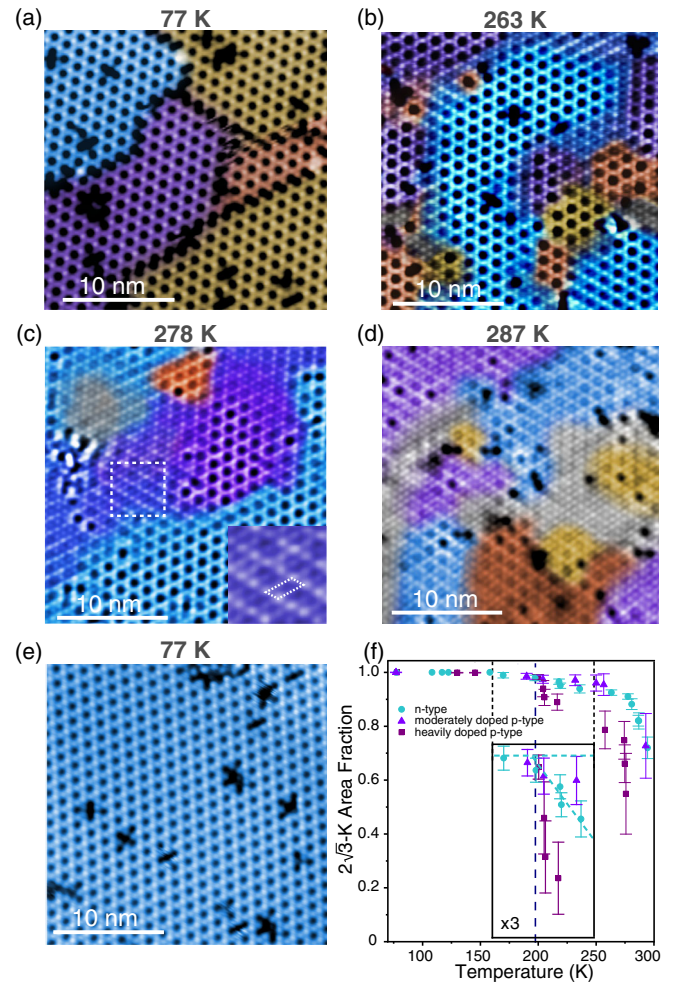


FIG. 3. Temperature dependent topography of the $2\sqrt{3}$ -K structure on *n*-type Si(111). The sample was grown at 120 K, cooled to and imaged at 77 K (a), then slowly warmed to room temperature (b)–(d), and finally cooled down to 77 K (e). Four out-of-phase domains of the $2\sqrt{3}$ -K structure are displayed in different colors; a different $(\sqrt{3} \times \sqrt{3})R30^\circ$ phase that appears only above 200 K is in gray. The inset of panel (c) is an enlarged image of local $(\sqrt{3} \times 2\sqrt{3})$ ordering within the dashed white square [the $(\sqrt{3} \times 2\sqrt{3})$ UC is marked by a dashed rhomboid in the inset]. All images were obtained with a sample bias of -1.5 V and 30 pA current. (f) Area fraction of the low-temperature $2\sqrt{3}$ -K phase for three different substrates. Nucleation of high-temperature domains and concomitant loss of long-range $2\sqrt{3}$ -K order starts at 200 K. The inset shows that the nucleation temperature is independent of the substrate doping level. However, the transition proceeds a bit faster on the heavily doped *p*-type substrate.

temperatures using the FIREBALL code [38]. We used a basis set of numerical atomiclike orbitals that yields a good description for the K/Sn/Si(111) system [15]. The simulations are performed using a $(2\sqrt{3} \times 2\sqrt{3})$ UC and thus cannot account for the complex domain structures in Fig. 3. However, they do provide insights into the K distribution and Sn adatom relaxations at different

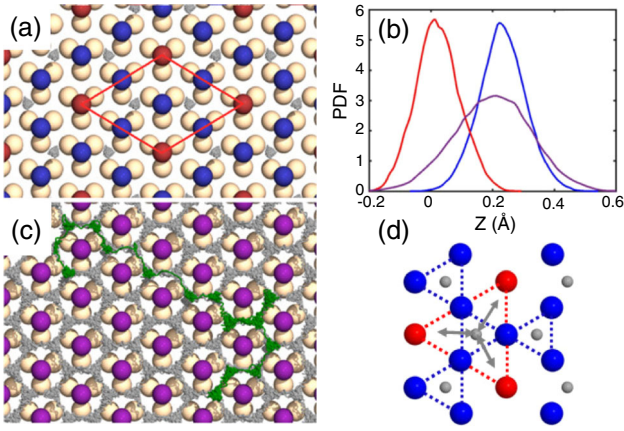


FIG. 4. Atomic dynamics in the K/Sn layer. (a),(c),(d) Top view of the $2\sqrt{3}$ -K surface. Blue and red marbles represent the Sn-up and Sn-down atoms, respectively. Beige marbles represent the Si atoms below. Gray lines track the motion of the K atoms at 77 K (a) and 300 K (c). The green line in (c) follows the trajectory of a single K atom along a 300 ps DFT-MD simulation [38]. At 300 K all Sn adatoms are equivalent [purple marbles in (c)]. (b) Probability distribution functions for the Sn-up (blue) and Sn-down (red) adatom heights at 77 K, and for the Sn atoms at 300 K (purple); $z = 0.0$ Å is the height of the Sn-down atoms in the $2\sqrt{3}$ -K structure. (d) Schematic illustration of the short-range positional fluctuations of the K atoms to neighboring T_4 sites.

temperatures, elucidating the interplay between the melting of the K sublattice and the charge-order transition.

At 77 K, the system exhibits long-range ($2\sqrt{3} \times 2\sqrt{3}$) order. The DFT-MD simulations show K atoms “rattling” around their stable positions at the T_4 sites inside the chained triangles of the kagome lattice, see Fig. 4(a). Meanwhile, the Sn atoms oscillate around their up or down equilibrium positions, shown by their height distributions in Fig. 4(b). At higher temperatures [Figs. 4(c) and 4(d)], K atoms start jumping to neighboring potential wells defined by open T_4 sites on the Si surface [Fig. 4(d)]. In total, there are eight such sites per ($2\sqrt{3} \times 2\sqrt{3}$) UC [Fig. 1(d)], and 28 possible K configurations. Four of those correspond to the $2\sqrt{3}$ -K domains in Fig. 3(a), which remain stable up to at least 200 K [Fig. 3(f)].

To understand how the gradual reduction of the HOMO-LUMO gap might be related to these positional fluctuations, we performed plane-wave DFT calculations for a large ($4\sqrt{3} \times 4\sqrt{3}$) UC in which one K atom is displaced towards a neighboring T_4 site [Fig. 4(d)]. In this “snapshot” configuration, the K atom has moved away from one Sn-up atom (say Sn_1) of the kagome lattice, landing next to a Sn-down atom (Sn_2) of the triangular lattice [15]. The DFT results show that this induces a downward displacement ($\Delta z \approx 0.04$ Å) of Sn_1 and an upward displacement ($\Delta z \approx 0.07$ Å) of Sn_2 ; the corresponding DB states move into the gap, as indicated by the red dotted spectrum in Fig. 2(b).

The apparent downshift of the LUMO in Fig. 2(a) can be attributed to the emergence of the Sn_2 state on the low-energy side of the LUMO. Indeed, this is evident from a fitting of the experimental LUMO spectra (not shown) and from an eyeball inspection of, e.g., the 175 K spectrum. The emergence of the Sn_1 state on the HOMO side is less noticeable. This can be attributed to the 3 : 1 LDOS ratio of the HOMO and LUMO manifolds in the $2\sqrt{3}$ -K ground state. Accordingly, the spectral weight transfers to the Sn_1 and Sn_2 states in the ($4\sqrt{3} \times 4\sqrt{3}$) snapshot configuration is 1/12 and 1/4, respectively. As the number of short-range hopping events increases with temperature, the LUMO shoulder becomes increasingly pronounced [Fig. 2(c)].

The energy barrier for the K adatom jump from its original location to the neighboring T_4 site is 0.16 eV. An additional jump requires 0.20 eV, while the reverse jump to the original location only requires 0.09 eV. Thus, at $T = 150$ K it is much more likely that the shifted K atom returns to its original site, hence the K fluctuations at 150 K are indeed short ranged. These barriers are estimated by fixing the x - y coordinates of the jumping K atom at the intermediate point between the two energy minima and relaxing the other coordinates of the system.

Above 200 K, K atoms start visiting the other 24 adatom configurations in the ($2\sqrt{3} \times 2\sqrt{3}$) UC. In all these configurations, Sn adatoms align in ($\sqrt{3} \times 2\sqrt{3}$) rows [Fig. 3(c), inset]. The computed adatom height in the upper row is identical to that of the up atoms of the $2\sqrt{3}$ -K phase while the Sn atoms in the lower row are only ~ 0.10 Å below, in excellent agreement with the measured height difference of 0.08 Å in STM. Hence, the buckling distortion of the charge-ordered $2\sqrt{3}$ -K phase is greatly reduced due to the upward relaxation of the down atoms of the triangular Sn sublattice. This can be viewed as a displacive transition: at low T the Sn up and down atoms oscillate around their equilibrium positions (with a theoretical height difference of 0.23 Å), while at high T the Sn down atoms oscillate around a new vertical position ≈ 0.13 Å above the original one.

At 300 K, the K sublattice is molten [Fig. 4(c)] and the K atoms visit all K configurations [39]. Meanwhile, Sn adatoms fluctuate between different ($\sqrt{3} \times 2\sqrt{3}$) configurations, and the distinction between Sn up and down is totally lost [Fig. 4(b)]. The system ultimately transforms into a ($\sqrt{3} \times \sqrt{3}$) phase with a total collapse of the charge ordering. This final step is typical of an order-disorder transition where the disorder refers to dynamical fluctuations between different ($\sqrt{3} \times 2\sqrt{3}$) structures [10,40,41].

The following picture emerges. The melting of the $2\sqrt{3}$ -K charge-ordered condensate starts at about 130 K and proceeds through two intermediate regimes. The first one is characterized by short-range positional fluctuations of the K atoms, illustrated in Fig. 4(d). These are mostly nearest-neighbor hopping events where the K atoms always

return to their original sites, thus maintaining long-range ($2\sqrt{3} \times 2\sqrt{3}$) order up to 200 K. These fluctuations are accompanied by up-down relaxations of the neighboring Sn atoms and become more prominent with increased temperature, inducing the gradual reduction of the HOMO-LUMO gap.

The second intermediate regime starts at 200 K, the nucleation temperature of the ($\sqrt{3} \times 2\sqrt{3}$) and ($\sqrt{3} \times \sqrt{3}$) domains. Here, K atoms diffuse over longer distances. The formation of the ($\sqrt{3} \times 2\sqrt{3}$) domains involves a displacive mechanism while the formation of the ($\sqrt{3} \times \sqrt{3}$) domains involves an additional order-disorder transition at higher temperature. Experimentally, the $2\sqrt{3}$ -K, ($\sqrt{3} \times 2\sqrt{3}$), and ($\sqrt{3} \times \sqrt{3}$) structures all coexist above 200 K. This is typical of a preempted first order melting transition on a rigid substrate, where solid and liquid phases can coexist over a wide temperature range, due to long-range elastic interactions between the various domains [42].

The present scenario is somewhat reminiscent of the Kosterlitz, Thouless, Halperin, Nelson, and Young theory for 2D melting [1–3]. In this theory, 2D melting proceeds via an intermediate quasiordered “hexatic” phase, characterized by exponential decay of positional order correlations and power law decay of orientational correlations. Advanced simulations on simplified model systems suggest that the solid-hexatic transition is continuous while the hexatic liquid transition can be first order [4]. Both transitions arise from the subsequent unbinding of topological defects such as paired dislocations and formation of free disclinations. The current situation is more complicated due to the presence of a substrate, absence of sixfold rotational order, and the coupling to the charge-order transition in the host lattice. Yet the microscopic multistep melting scenario discussed here presents interesting similarities (and differences) with the two-step continuous-discontinuous melting transition mentioned above [4]. Whether or not the coexisting periodicities and domain walls are topologically entangled [16] and/or whether topological excitations play a role in this novel melting phenomenon remains to be determined.

The experimental work was funded by the National Science Foundation under Grant No. DMR 1410265. T. S. S. acknowledges the Center for Materials Processing, a Tennessee Higher Education Commission supported Accomplished Center of Excellence, for financial support. The theoretical work was funded by Spanish Ministry of Science and Innovation under Projects No. MAT2017-88258-R and No. CEX2018-000805-M (“María de Maeztu” Programme for Units of Excellence in R&D). The authors acknowledge the computer resources at Cibeles and the technical support provided by the Centro de Computación Científica-UAM (CCC-UAM), Projects No. FI-2019-0028 and No. BIOFAST.

*These authors contributed equally to this work.

†Corresponding author.

hanno@utk.edu

- [1] J. M. Kosterlitz and D. J. Thouless, *J. Phys. C* **6**, 1181 (1973).
- [2] B. I. Halperin and D. R. Nelson, *Phys. Rev. Lett.* **41**, 121 (1978).
- [3] A. P. Young, *Phys. Rev. B* **19**, 1855 (1979).
- [4] E. P. Bernard and W. Krauth, *Phys. Rev. Lett.* **107**, 155704 (2011).
- [5] V. N. Ryzhov, E. E. Tareyeva, Yu D. Fomin, and E. N. Tsiok, *Phys. Usp.* **60**, 857 (2017).
- [6] L. D. Landau and E. M. Lifshitz, *Statistical Physics*, 3rd ed. (Pergamon Press Ltd, New York, 1980).
- [7] R. M. White and T. H. Geballe, *Long-Range Order in Solids* (Academic Press, New York, 1979).
- [8] V. Naden Robinson, H. Zong, G. J. Ackland, G. Woolman, and A. Hermann, *Proc. Natl. Acad. Sci. U.S.A.* **116**, 10297 (2019).
- [9] J. D. Fan, G. Reiter, and S. C. Moss, *Phys. Rev. Lett.* **64**, 188 (1990).
- [10] W. Qiu, L. Xi, P. Wei, X. Ke, J. Yang, and W. Zhang, *Proc. Natl. Acad. Sci. U.S.A.* **111**, 15031 (2014).
- [11] S. Modesti, L. Petaccia, G. Ceballos, I. Vobornik, G. Panaccione, G. Rossi, L. Ottaviano, R. Larciprete, S. Lizzit, and A. Goldoni, *Phys. Rev. Lett.* **98**, 126401 (2007).
- [12] G. Li, P. Höpfner, J. Schäfer, C. Blumenstein, S. Meyer, A. Bostwick, E. Rotenberg, R. Claessen, and W. Hanke, *Nat. Commun.* **4**, 1620 (2013).
- [13] F. Ming, S. Johnston, D. Mulugeta, T. S. Smith, P. Vilmercati, G. Lee, T. A. Maier, P. C. Snijders, and H. H. Weitering, *Phys. Rev. Lett.* **119**, 266802 (2017).
- [14] F. Ming, D. Mulugeta, W. Tu, T. S. Smith, P. Vilmercati, G. Lee, Y.-T. Huang, R. D. Diehl, P. C. Snijders, and H. H. Weitering, *Nat. Commun.* **8**, 14721 (2017).
- [15] See the Supplemental Material at <http://link.aps.org/supplemental/10.1103/PhysRevLett.124.097602> for coverage calibration and registry of the K atoms, growth morphologies on different substrates, and theoretical details. The Supplemental Material includes Refs. [16–28] that are not referred to in the main text.
- [16] G. Gye, E. Oh, and H. W. Yeom, *Phys. Rev. Lett.* **122**, 016403 (2019).
- [17] A. Goldoni and S. Modesti, *Phys. Rev. Lett.* **79**, 3266 (1997).
- [18] S. Yi, F. Ming, Y.-T. Huang, T. S. Smith, X. Peng, W. Tu, D. Mulugeta, R. D. Diehl, P. C. Snijders, J.-H. Cho, and H. H. Weitering, *Phys. Rev. B* **97**, 195402 (2018).
- [19] L. Chaput, C. Tournier-Colletta, L. Cardenas, A. Tejada, B. Kierren, D. Malterre, Y. Fagot-Revurat, P. Le Fèvre, F. Bertran, A. Taleb-Ibrahimi, D. G. Trabada, J. Ortega, and F. Flores, *Phys. Rev. Lett.* **107**, 187603 (2011).
- [20] J. P. Perdew, K. Burke, and M. Ernzerhof, *Phys. Rev. Lett.* **77**, 3865 (1996).
- [21] S. Goedecker, M. Teter, and J. Hutter, *Phys. Rev. B* **54**, 1703 (1996).
- [22] C. Hartwigsen, S. Goedecker, and J. Hutter, *Phys. Rev. B* **58**, 3641 (1998).
- [23] M. J. Monkhorst and J. D. Pack, *Phys. Rev. B* **13**, 5188 (1976).

- [24] A. D. Becke, *Phys. Rev. A* **38**, 3098 (1988).
- [25] C. Lee, W. Yang, and R. G. Parr, *Phys. Rev. B* **37**, 785 (1988).
- [26] M. A. Basanta, Y. J. Dappe, P. Jelínek, and J. Ortega, *Comput. Mater. Sci.* **39**, 759 (2007).
- [27] J. M. Blanco, C. González, P. Jelínek, J. Ortega, F. Flores, and R. Pérez, *Phys. Rev. B* **70**, 085405 (2004).
- [28] C. González, P. C. Snijders, J. Ortega, R. Pérez, F. Flores, S. Rogge, and H. H. Weiering, *Phys. Rev. Lett.* **93**, 126106 (2004).
- [29] M.-C. Desjonqueres and D. Spanjaard, *Concepts in Surface Physics* (Springer-Verlag, Berlin, 1993).
- [30] J. Avila, A. Mascaraque, E. G. Michel, M. C. Asensio, G. Le Lay, J. Ortega, R. Perez, and F. Flores, *Phys. Rev. Lett.* **82**, 442 (1999).
- [31] J. M. Carpinelli, H. H. Weiering, E. W. Plummer, and R. Stumpf, *Nature (London)* **381**, 398 (1996).
- [32] J. M. Carpinelli, H. H. Weiering, M. Bartkowiak, R. Stumpf, and E. W. Plummer, *Phys. Rev. Lett.* **79**, 2859 (1997).
- [33] P. Giannozzi *et al.*, *J. Phys. Condens. Matter* **21**, 395502 (2009).
- [34] J. A. Stroschio, R. M. Feenstra, and A. P. Fein, *Phys. Rev. Lett.* **57**, 2579 (1986).
- [35] J. P. Perdew, M. Ernzerhof, and K. Burke, *J. Chem. Phys.* **105**, 9982 (1996).
- [36] C. Adamo and V. Barone, *J. Chem. Phys.* **110**, 6158 (1999).
- [37] STS spectra at higher temperatures tend to be noisier in the occupied states, this produces small fluctuations of the HOMO position after data averaging and subsequent differentiation.
- [38] J. P. Lewis, P. Jelínek, J. Ortega, A. A. Demkov, D. G. Trabada, B. Haycock, H. Wang, G. Adams, J. K. Tomfohr, E. Abad, H. Wang, and D. A. Drabold, *Phys. Status Solidi B* **248**, 1989 (2011).
- [39] Since these are periodic DFT-MD simulations, when one K atom is leaving the $(2\sqrt{3} \times 2\sqrt{3})$ unit cell in one side, another K atom is entering the unit cell on the opposite side. In Figs. 4(a) and 4(c) we show the motion of the K atoms of the central and surrounding unit cells.
- [40] C. González, F. Flores, and J. Ortega, *Phys. Rev. Lett.* **96**, 136101 (2006).
- [41] D. G. Trabada, J. I. Mendieta-Moreno, D. Soler-Polo, F. Flores, and J. Ortega, *Appl. Surf. Sci.* **479**, 260 (2019).
- [42] J. B. Hannon, F. J. Meyer zu Heringdorf, J. Tersoff, and R. M. Tromp, *Phys. Rev. Lett.* **86**, 4871 (2001).